# Multiparametric MRI in the Diagnosis of Prostate Cancer: Physical Foundations, Limitations, and Prospective Advances of Diffusion-Weighted MRI

## Multiparametrische MRT in der Diagnose des Prostatakarzinoms: Physikalische Grundlagen, Limitationen und potenzielle Fortschritte der diffusionsgewichteten MRT

Authors

Barbara Daria Wichtmann[1], Frank Gerrit Zöllner[2], Ulrike Irmgard Attenberger[1], Stefan O. Schönberg[3]

Affiliations

1 Department of Diagnostic and Interventional Radiology, University Hospital Bonn, Germany
2 Computer Assisted Clinical Medicine, Mannheim Institute for Intelligent Systems in Medicine, Medical Faculty Mannheim, Heidelberg University, Mannheim, Germany
3 Department of Radiology and Nuclear Medicine, University Medical Center Mannheim, Germany

Key words

advanced diffusion-weighted imaging models, non-gaussian diffusion-weighted imaging models, compartment diffusion-weighted imaging models, MR-diffusion < METHODS & TECHNIQUES, multiparametric MRI, prostate cancer

**received** 02.04.2020
**accepted** 18.09.2020
**published online** 10.12.2020

Bibliography

Fortschr Röntgenstr 2021; 193: 399–409
**DOI** 10.1055/a-1276-1773
**ISSN** 1438-9029

Georg Thieme Verlag KG, Rüdigerstraße 14, 70469 Stuttgart, Germany

Correspondence

Barbara Daria Wichtmann
Radiology, University Hospital Bonn, Venusberg-Campus 1, 53127 Bonn, Germany
Tel.: +49/2 28/28 71 58 71
Fax: +49/2 28/28 71 60 93
barbara.wichtmann@ukbonn.de

### ZUSAMMENFASSUNG

**Hintergrund** Die diffusionsgewichtete MRT-Bildgebung (DWI) ist wesentlicher Bestandteil der multiparametrischen MRT zur Diagnostik und Beurteilung des Prostatakarzinoms (PCa). In den letzten 2 Jahrzehnten wurden diverse Modelle entwickelt, um das DWI-Signal quantitativ mit mikrostrukturellen Charakteristiken des Prostatagewebes in Beziehung zu setzen. Der einfachste, heute als klinischer Standard etablierte Ansatz (apparenter Diffusionskoeffizient, ADC) beschreibt eine monoexponentielle Abnahme des DWI-Signals. Obwohl zahlreiche Studien eine inverse Korrelation von ADC-Werten mit dem Gleason-Score zeigen konnten, weist dieses Modell eine geringe Spezifität auf und basiert auf einer Wasserdiffusionsdynamik, die im menschlichen Gewebe nicht zutrifft. Ziel dieses Artikels ist es, die biophysikalischen Grenzen des Standard-DWI-Modells zu erklären und das Potenzial komplexerer, weiterentwickelter DWI-Modelle aufzuzeigen.

**Methode** Bei diesem Artikel handelt es sich um eine Übersichtsarbeit auf der Basis einer selektiven Literaturaufarbeitung.

**Ergebnisse** Vorgestellt werden die 4 phänomenologischen DWI-Modelle Diffusion Tensor Imaging, Intravoxel Incoherent Motion, Biexponential Model und Diffusion Kurtosis Imaging, deren Parameter möglicherweise einen Mehrwert in der PCa-Diagnostik darstellen, jedoch in aktuellen Studien eine variierende statistische Signifikanz hinsichtlich der Detektion und Charakterisierung des PCa zeigen. Phänomenologischen Modellparametern mangelt es an Spezifität, was die Entwicklung von deskriptiveren Gewebemodellen motivierte, die mikrostrukturelle Merkmale direkt mit dem Signal in Zusammenhang bringen. Abschließend stellen wir 2 dieser strukturellen Modelle vor, d. h. das VERDICT (Vascular, Extracellular and Restricted Diffusion for Cytometry in Tumors) sowie das RSI (Restriction Spectrum Imaging)-Modell. Beide zeigten in ersten Studien vielversprechende Ergebnisse bezüglich der Charakterisierung und Prognose des PCa.

**Schlussfolgerung** Neuere Entwicklungen der DWI-Techniken lassen eine zunehmende Genauigkeit und spezifischere Aussagen über mikrostrukturelle Veränderungen des PCa erwarten. Weitere Studien sind erforderlich, um ein standardisiertes DWI-Protokoll für die Diagnostik des PCa zu etablieren.

**Kernaussagen:**

- Die DWI ist für die mpMRI-Untersuchung zur Diagnose des PCa von großer Bedeutung.
- Obwohl von hohem klinischen Wert, weist das ADC-Modell eine geringe Spezifität auf und vereinfacht die Gewebekomplexität zu stark.

- Zur Beschreibung des DWI-Signals wurden weitergehende phänomenologische und strukturelle Modelle entwickelt.
- Phänomenologische Modelle können zu einer Verbesserung der Diagnostik führen, liefern jedoch inkonsistente Ergebnisse hinsichtlich der Beurteilung des PCa.
- Strukturelle Modelle zeigen in ersten Studien vielversprechende Ergebnisse hinsichtlich der Charakterisierung des PCa auf.

## ABSTRACT

**Background** Diffusion-weighted imaging (DWI) is an essential component of the multiparametric MRI exam for the diagnosis and assessment of prostate cancer (PCa). Over the last two decades, various models have been developed to quantitatively correlate the DWI signal with microstructural characteristics of prostate tissue. The simplest approach (ADC: apparent diffusion coefficient) – currently established as the clinical standard – describes monoexponential decay of the DWI signal. While numerous studies have shown an inverse correlation of ADC values with the Gleason score, the ADC model lacks specificity and is based on water diffusion dynamics that are not true in human tissue. This article aims to explain the biophysical limitations of the standard DWI model and to discuss the potential of more complex, advanced DWI models.

**Methods** This article is a review based on a selective literature review.

**Results** Four phenomenological DWI models are introduced: diffusion tensor imaging, intravoxel incoherent motion, biexponential model, and diffusion kurtosis imaging. Their parameters may potentially improve PCa diagnostics but show varying degrees of statistical significance with respect to the detection and characterization of PCa in current studies. Phenomenological model parameters lack specificity, which has motivated the development of more descriptive tissue models that directly relate microstructural features to the DWI signal. Finally, we present two of such structural models, i. e. the VERDICT (Vascular, Extracellular, and Restricted Diffusion for Cytometry in Tumors) and RSI (Restriction Spectrum Imaging) model. Both have shown promising results in initial studies regarding the characterization and prognosis of PCa.

**Conclusion** Recent developments in DWI techniques promise increasing accuracy and more specific statements about microstructural changes of PCa. However, further studies are necessary to establish a standardized DWI protocol for the diagnosis of PCa.

**Key Points:**

- DWI is paramount to the mpMRI exam for the diagnosis of PCa.
- Though of clinical value, the ADC model lacks specificity and oversimplifies tissue complexities.
- Advanced phenomenological and structural models have been developed to describe the DWI signal.
- Phenomenological models may improve diagnostics but show inconsistent results regarding PCa assessment.
- Structural models have demonstrated promising results in initial studies regarding PCa characterization.



**Citation Format**

- Wichtmann BD, Zöllner FG, Attenberger UI et al. Multiparametric MRI in the Diagnosis of Prostate Cancer: Physical Foundations, Limitations, and Prospective Advances of Diffusion-Weighted MRI. Fortschr Röntgenstr 2021; 193: 399–409


## Introduction

Prostate cancer (PCa) is the most common cancer in men, accounting for 22.7 % of all diagnosed cancers (excluding non-melanoma skin cancer), and is the second leading cause of cancer death in Germany [1]. Due to demographic change, both the incidence and prevalence are expected to increase continuously. Overall, about 40 % of the male population in western industrialized countries are at risk of developing PCa during their lifetime, of which about 10 % become symptomatic and 3 % die [2, 3]. This demographic development must be taken into account in the diagnosis, treatment, and follow-up care of PCa. Conventional diffusion-weighted imaging (DWI) was shown to add incremental value to T2-weighted (T2w) magnetic resonance imaging (MRI) in the detection and localization of PCa, making it a key component of the prostate multiparametric MRI (mpMRI) exam [4–6].

In this review, we want to provide a brief background on mpMRI and the importance of DWI. We will describe how the observed diffusion phenomena can be measured with DWI and review the basic physical principles governing diffusion within tissue. Based on the above, we aim to explain the biophysical limitations of the currently used DWI model in the standard mpMRI exam and outline the potential of advanced signal modeling techniques for an improved assessment and local staging of PCa.

## Diagnostics and the importance of mpMRI

PCa is usually suspected on the basis of digital rectal examination and/or prostate-specific antigen (PSA) levels [2]. The use of PSA as a screening tool followed by systematic transrectal ultrasound (TRUS)-guided biopsy has led to increased and earlier detection of PCa [2]. This entails the risk of overdiagnosis and, consequently, overtherapy. Additionally, systematic biopsy alone fails to detect up to 20 % of significant carcinomas [7]. Today, mpMRI, consisting of T2w, DW, and dynamic contrast-enhanced (DCE) imaging, has shown substantial value in the staging, detection, localization, characterization, risk stratification, surveillance, and assessment of suspected recurrence of PCa [6]. Data from systematic reviews and diagnostic studies indicate that a combination of MRI-assisted, targeted plus systematic biopsy achieves much better detection rates than the respective methods alone [2, 8]. In the 4-M study, while comparable detection rates of clinically significant

PCa were achieved between systematic TRUS-guided biopsy and MRI targeted biopsy, Leest at al. were able to show that biopsy-naïve men can benefit from MRI as fewer indolent cancers are detected and biopsy may be omitted in half of the patients without affecting the detection of clinically significant PCa [9]. According to the German S3 guidelines [2], negative systematic biopsies in primary diagnostics should be followed by MRI and, if necessary, targeted plus systematic biopsy in case of continued suspicion of PCa. On this basis, further imaging or invasive interventions are determined. In addition, it is recommended to perform an MRI examination before including patients in active surveillance.

To standardize the evaluation of PCa by MRI, the American College of Radiology, European Society of Urogenital Radiology, and the AdMeTech Foundation established a scoring system, i. e., Prostate Imaging Reporting and Data System (PI-RADS). PI-RADS v2.1 assessment utilizes a score from 1 (very low) to 5 (very high) based on the likelihood that a combination of mpMRI findings on T2w/DWI/DCE correlates with the presence of clinically significant PCa [4, 5].

## The impact of DWI

Owing to its unique sensitivity to the molecular self-diffusion of water, DWI is a powerful tool to noninvasively study the microstructural properties of biological tissue in vivo [10]. DWI is paramount to the prostate mpMRI exam. It is the primary determining sequence to assign the PI-RADS score for lesions within the peripheral zone where PCa arises in about 85 % of cases [4, 5, 11].

Over the last two decades various theoretical models have been developed that quantitively connect the DWI signal to salient features of tissue microstructure. The simplest approach to describe the attenuated DWI signal is in terms of the so-called apparent diffusion coefficient (*ADC*) which today has become established as the clinical standard [12]. Numerous studies were able to demonstrate an inverse correlation of *ADC* values with the Gleason score and tumor proliferation markers (Ki-67) [13]. Still, there is a substantial overlap of *ADC* values within healthy, cancerous, and inflamed (e. g. prostatitis, post-biopsy inflammation) prostate tissue.

Recent advances in MRI have led to the development of high-performance gradient systems, stronger magnets and improved coil technology that allow for shorter diffusion/echo times and an improved signal-to-noise ratio (SNR). This progress enables the investigation of innovative, advanced DWI models to improve PCa assessment performance [4].

## Principles of DWI

The foundation of basically all modern DWI sequences is the pulsed gradient spin echo technique developed by Stejskal and Tanner in 1965 [14]. Diffusion sensitivity is achieved by spatially dependent, strong magnetic field gradient pulses that are applied before and after the inversion pulse of a 90°–180° radiofrequency pulse combination. Diffusion along the gradient direction causes signal attenuation (▶ **Fig. 1**).

Various DWI models have been developed to either mathematically describe this signal attenuation reliably as a function of increasing diffusion weighting, i. e. phenomenological, or to predict this signal attenuation based on calculated/simulated diffusion dynamics in structural compartments, i. e. structural [15].

## Physical principles of diffusion within tissue

Diffusion within biological tissue is a highly intricate process, particularly within the structural complexities of cancerous prostate tissue. In a greatly simplified tissue model, we differentiate three modes of diffusion: free, hindered, and restricted (▶ **Fig. 2**, [10, 16–18]).

### Free diffusion

Free water diffusion refers to the random (Brownian) motion of water molecules driven by thermal agitation in an isotropic, homogeneous environment of infinite extent. The displacement distribution of diffusing free water molecules after a given time interval is Gaussian and described by Einstein's equation [19]. The diffusion distance $s = \sqrt{2D\Delta}$ increases linearly with the square root of diffusion time (Δ) with the diffusion coefficient *D* as a constant slope.

### Hindered diffusion

Hindered water diffusion refers to the diffusion process within the extracellular space where water molecules are hindered in their free movement by impermeable cellular barriers which they must bypass [10]. The extracellular water compartment is not restricted, i. e. the diffusion space is infinite. Thus, water molecules can principally diffuse over very long distances and the distribution of squared displacements takes a Gaussian form. For very short Δ, the diffusion paths of hindered particles appear to be free. For longer Δ, the diffusion distance still increases linearly with the square root of Δ, but with a reduced slope [17].

### Restricted diffusion

Restricted diffusion refers to the diffusion process within enclosed, impermeable compartments, such as the intracellular space [10]. Diffusion within the intracellular compartment is confined by cell membranes. While intracellular water molecules initially diffuse freely, they eventually hit the cell boundaries with increasing Δ. Hence, the mean-squared displacement of intracellular molecules does not scale linearly with Δ, but ultimately levels off when the dimensions of the restricting compartment are reached [17]. Thus, the displacement distribution of diffusion-restricted water molecules is non-Gaussian and the measured *ADC* decreases with Δ [10].

### Isotropic vs. anisotropic diffusion

While diffusion in homogeneous environments is the same in every direction, i. e. isotropic, diffusion within biological tissue varies along different directions, i. e. anisotropic. Thus, anisotropic diffusion environments cannot be described by a single diffusion coefficient.

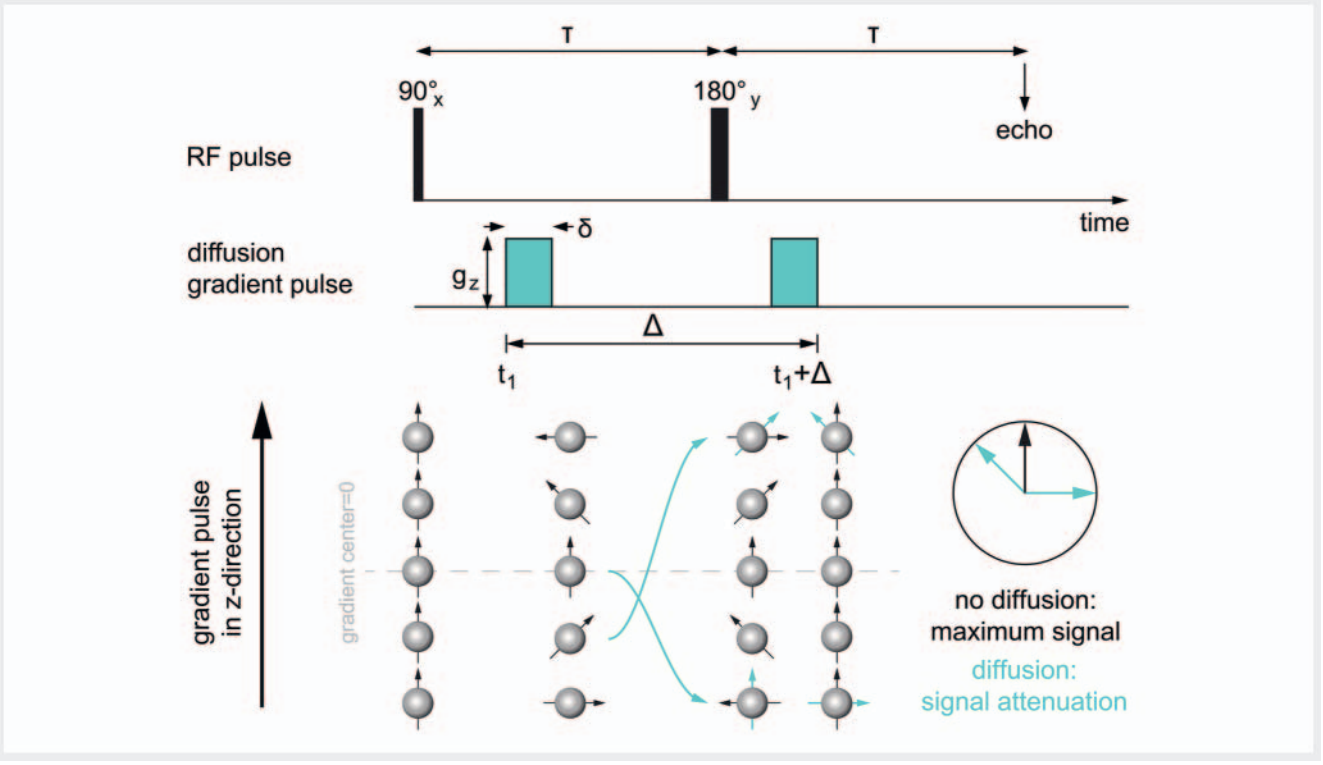


▶ **Fig. 1** A schematic, graphical representation of the Stejskal-Tanner pulsed gradient spin echo experiment and how it measures diffusion. The first diffusion gradient pulse of magnitude g and duration δ induces a phase shift for spins based on their position along the axis of the gradient. The identical second gradient pulse applied after a certain time Δ (so-called diffusion time) on the other side of the 180° inversion radiofrequency (RF) pulse leads to a perfect rephasing and maximum signal in case of no diffusion. Translation along the gradient direction, however, results in a phase error and signal loss which increases with greater displacement. Increasing diffusion weighting can be achieved by applying stronger gradients, extending the gradient duration or by lengthening the diffusion time. A combination of these factors yields the diffusion weighting factor b, which can be expressed as $b = (\gamma\delta g)^2 (\Delta - \delta/3)$, where γ is the gyromagnetic ratio.

▶ **Abb. 1** Eine schematische, grafische Darstellung der Stejskal-Tanner Pulsed Gradient Spin Echo Sequenz und ihrer Messung der Diffusion. Der erste Diffusionsgradientenimpuls der Stärke g und Dauer δ induziert eine Phasenverschiebung der Spins basierend auf ihrer Position entlang der Gradientenachse. Der identische zweite Gradientenimpuls, der nach einer bestimmten Zeit Δ (sog. Diffusionszeit) nach dem 180° Inversions-Radiofrequenzimpuls (RF) angelegt wird, führt bei ausbleibender Diffusion zu einer perfekten Rephasierung und einem maximalen Signal. Diffusion entlang der Gradientenrichtung führt jedoch zu einem Phasenfehler und Signalverlust, der mit zunehmender Diffusion wächst. Eine größere Diffusionswichtung kann durch stärkere Gradienten, längere Gradientendauern oder höhere Diffusionszeiten erreicht werden. Eine Kombination dieser Faktoren ergibt den Diffusionswichtungsfaktor b, der als $b = (\gamma\delta g)^2 (\Delta - \delta/3)$ ausgedrückt werden kann, wobei γ das gyromagnetische Verhältnis darstellt.

## Phenomenological DWI models in PCa

### ADC model – current clinical standard

PCa assessment utilizing clinical DWI methods is currently almost exclusively based on the simplest possible Gaussian diffusion model [12]. Mathematically, this can be expressed as monoexponential decay of the DWI signal *S* with increasing diffusion weighting *b* (▶ **Fig. 3**)

$$S(b) = S_0 e^{-b\,ADC}$$

where $S_0$ is the maximum signal intensity at $b = 0$ and $S(b)$ the measured signal intensity at a certain *b*-value.

The ADC model represents an oversimplification of the complex non-Gaussian diffusion behavior within tissue and misses biological specificity with respect to structural changes of cancerous tissue that define Gleason patterns as it depends on various histological features simultaneously [15]. Nevertheless, calculated *ADC* maps allow for a semi-quantitative assessment of gross variations in water diffusion dynamics. Various studies have shown that *ADC* values decrease with an increasing Gleason score, even though they substantially overlap within healthy, cancerous, and inflamed tissue, particularly in the central and transition zones [20–22]. A decrease in *ADC* values indicates reduced average water mobility which is commonly attributed to increased "cellularity". Yet, differences in compartment volumes of the prostate gland appear to be a more significant contributor to observed *ADC* differences than cellularity metrics. These differences include an increasing volume of epithelial cells with low diffusivity and correspondingly decreasing volumes of the fibromuscular stroma and lumen space with higher diffusivity [15, 23–25].

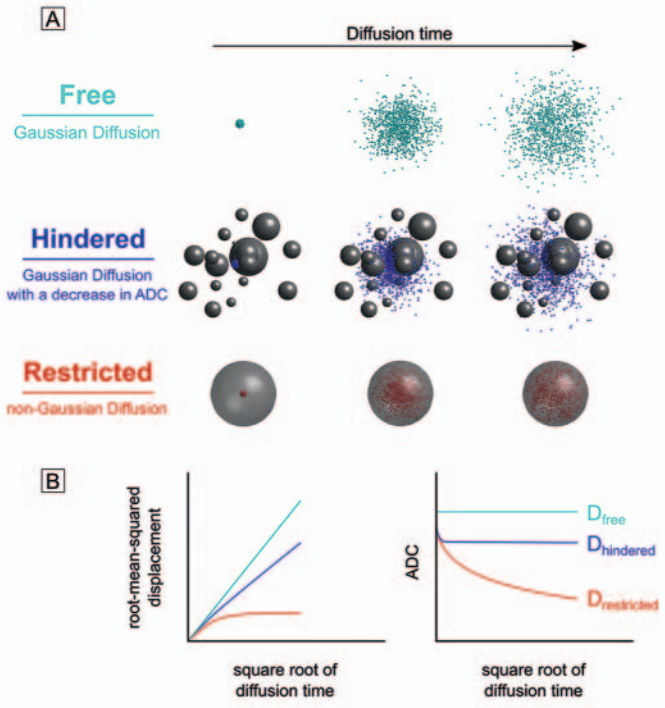


▶ **Fig. 2** Illustration of the physical principles of diffusion within tissue.
**A** *Free diffusion* occurs in an isotropic, homogeneous environment of infinite extent. **B** The root-mean-squared displacement of water molecules grows proportionally with the square root of diffusion time with the diffusion coefficient as a constant slope. At body temperature the free water diffusion coefficient measures approximately $D_{free} = 3\ \mu m^2/ms$. Following Einstein's equation, molecules therefore will travel approximately 15–25 µm during typical diffusion times of 40–100 ms in a DWI experiment.
**A** *Hindered diffusion* occurs within the extracellular space where water molecules have to diffuse around impermeable obstacles but are still not restricted with respect to the maximum distance they can travel. **B** The measured diffusion coefficient for hindered diffusion is diffusion time independent, except for very short diffusion times in which diffusion paths appear free. The degree of hindrance to diffusion within the extracellular space compared to free water diffusion can quantitatively be described by a tortuosity coefficient $\lambda = \sqrt{(D_{free}/D_{hindered})}$, where $D_{free}$ refers to the intrinsic free water diffusion coefficient and $D_{hindered}$ to the reduced, measured, apparent diffusion coefficient of the hindered compartment [16].
**A** *Restricted diffusion* occurs within the intracellular space where water molecules cannot diffuse beyond the cell dimensions. **B** Thus, the root-mean-squared displacement of intracellular molecules does not scale linearly with the square root of diffusion time, but ultimately levels off when the dimensions of the restricting compartment are reached [17]. The measured diffusion coefficient of the restricted compartment $D_{restricted}$ decreases with diffusion time. It should be noted that the permeability of cell membranes influences the diffusion characteristics [18]. However, exchange between the intra- and extracellular compartment is long (> 1 s) compared to typical diffusion times of 40–100 ms in a DWI experiment [10]. Finally, there is not one unique analytical expression to capture diffusion within the intracellular compartment. The measured DWI signal originating from restricted compartments is influenced by the size and shape of the cellular compartments as well as the conducted DWI experiment.

▶ **Abb. 2** Veranschaulichung der physikalischen Grundlagen der Diffusion im Gewebe.
**A** *Freie Diffusion* findet in einer isotropen, homogenen Umgebung von unendlicher Ausdehnung statt. **B** Die mittlere quadratische Verschiebung der Wassermoleküle wächst proportional mit der Quadratwurzel der Diffusionszeit, wobei der Diffusionskoeffizient die konstante Steigung beschreibt. Bei Körpertemperatur beträgt der Diffusionskoeffizient des freien Wassers ungefähr $D_{free} = 3\ \mu m^2/ms$. In Anlehnung an die Einstein'sche Gleichung bewegen sich die Moleküle daher bei typischen Diffusionszeiten von 40–100 ms in einem DWI-Experiment etwa 15–25 µm.
**A** *Gehinderte (engl. hindered) Diffusion* findet innerhalb des extrazellulären Raums statt, wo Wassermoleküle um undurchlässige Hindernisse herum diffundieren müssen, aber immer noch nicht in der maximalen Distanz, die sie zurücklegen können, eingeschränkt sind. **B** Der gemessene Diffusionskoeffizient für gehinderte Diffusion ist diffusionszeitunabhängig mit Ausnahme sehr kurzer Diffusionszeiten, für die die Diffusionspfade frei erscheinen. Der Grad der Diffusionshinderung innerhalb des extrazellulären Raums im Vergleich zur freien Wasserdiffusion kann quantitativ durch einen Tortuositätskoeffizienten $\lambda = \sqrt{(D_{free}/D_{hindered})}$ beschrieben werden, wobei $D_{free}$ sich auf den intrinsischen freien Wasserdiffusionskoeffizienten und $D_{hindered}$ auf den reduzierten, gemessenen scheinbaren Diffusionskoeffizienten des gehinderten Kompartiments bezieht [16].
**A** *Eingeschränkte Diffusion* tritt innerhalb des intrazellulären Raums auf, wo Wassermoleküle nicht über die Zellgrenzen hinaus diffundieren können. **B** Daher skaliert die mittlere quadratische Verschiebung der intrazellulären Wassermoleküle nicht linear mit der Quadratwurzel der Diffusionszeit, sondern flacht letztlich ab, wenn die Dimensionen des eingeschränkten Kompartiments erreicht werden [17]. Der gemessene Diffusionskoeffizient des eingeschränkten Kompartiments $D_{restricted}$ nimmt mit der Diffusionszeit ab. Es ist zu beachten, dass die Permeabilität der Zellmembranen die Diffusionseigenschaften beeinflusst [18]. Der Austausch zwischen dem intra- und extrazellulären Kompartiment ist jedoch lang (> 1 s) im Vergleich zu typischen Diffusionszeiten von 40–100 ms in einem DWI-Experiment [10]. Schließlich gibt es nicht einen einzigen analytischen Ausdruck zur Erfassung der Diffusion innerhalb des intrazellulären Kompartiments. Das gemessene DWI-Signal, das aus eingeschränkten Kompartimenten stammt, wird sowohl von der Größe und Form der zellulären Kompartimente als auch vom durchgeführten DWI-Experiment beeinflusst.

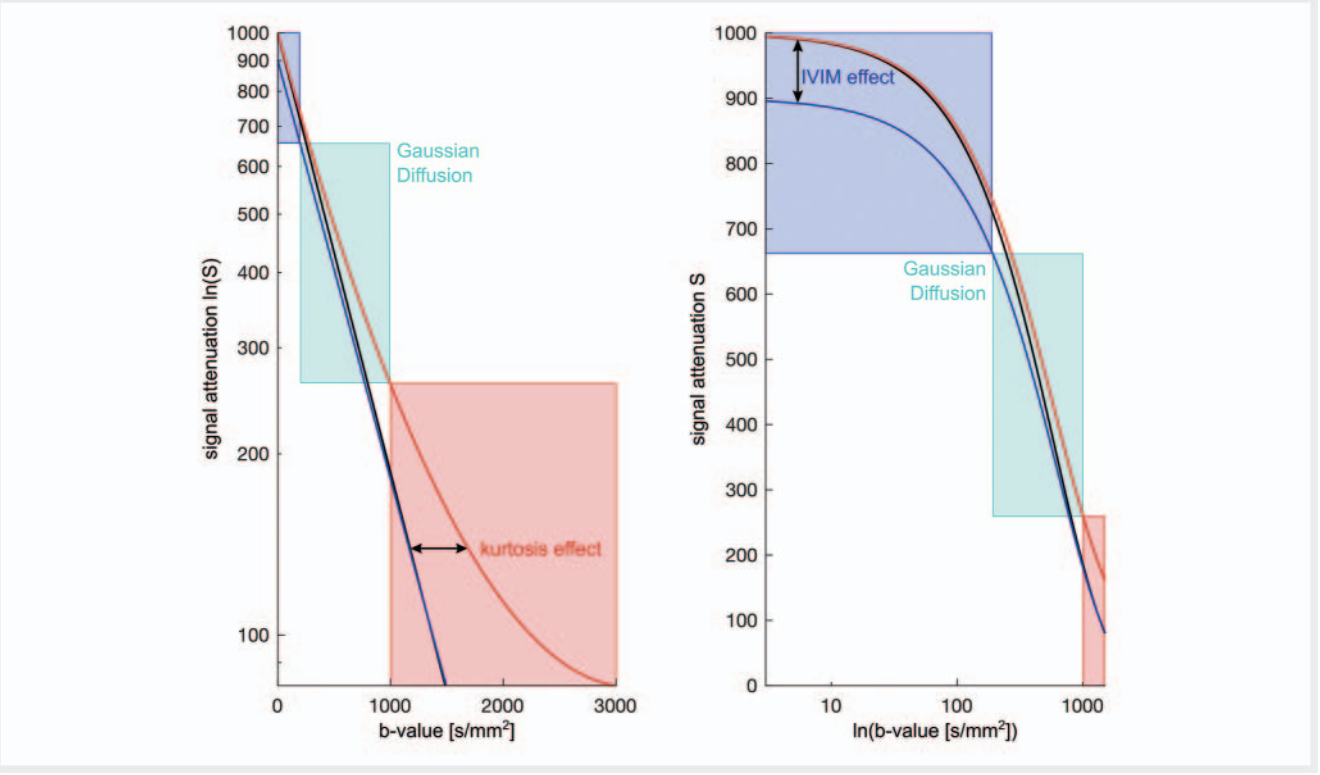


▶ **Fig. 3** DWI signal attenuation. The expected DWI signal attenuation assuming free Gaussian diffusion is plotted in black, depicting monoexponential decay with increasing diffusion weighting b. At very low b-values (≤ 200 s/mm²) IVIM effects (blue), i. e. blood microcirculation, contribute to the observed signal attenuation, leading to a deviation from the monoexponential model. At high b-values (≥ 1000 s/mm²) hindrance effects, particularly of cell membranes, evoke a non-Gaussian diffusion behavior, which causes a deviation from the straight line expected for free diffusion (red). One approach to quantify the deviation from the monoexponentional signal attenuation at high b-values assesses the kurtosis of the diffusion displacement probability distribution.

▶ **Abb. 3** Abschwächung des DWI-Signals. Die erwartete Signalabschwächung des DWI-Signals unter der Annahme freier Gaußscher Diffusion ist in schwarz dargestellt, wobei ein monoexponentieller Zerfall mit zunehmender Diffusionsgewichtung b beschrieben ist. Bei sehr niedrigen b-Werten (≤ 200 s/mm²) tragen IVIM-Effekte (blau), d.h. Blutmikrozirkulation, zur beobachteten Signalabschwächung bei, was zu einer Abweichung vom monoexponentiellen Modell führt. Bei hohen b-Werten (≥ 1000 s/mm²) verursachen Hinderungseffekte, insbesondere von Zellmembranen, ein nicht-gaußsches Diffusionsverhalten, wodurch es zu einer Abweichung von der für die freie Diffusion erwarteten Geraden kommt (rot). Ein Ansatz zur Quantifizierung der Abweichung von der monoexponentiellen Signalabschwächung bei hohen b-Werten bestimmt die Kurtosis der Wahrscheinlichkeitsverteilung der Diffusionsverschiebung.

## Diffusion tensor imaging (DTI)

DTI generalizes the ADC model to capture anisotropic diffusion observed in tissues with a high degree of structural order. To describe the orientation dependence of diffusion, a three-dimensional Gaussian model of molecular displacements is employed, which instead of the scalar *ADC* uses a symmetrical apparent diffusion tensor of water, ***D*** [26]. Generally, a principle Cartesian axis frame is used, thus

$$\boldsymbol{D} = \begin{bmatrix} D_{xx} & D_{xy} & D_{xz} \\ D_{xy} & D_{yy} & D_{yz} \\ D_{xz} & D_{yz} & D_{zz} \end{bmatrix}$$

where the three diagonal elements of ***D*** (i. e. $D_{xx}$, $D_{yy}$, $D_{zz}$) represent diffusion coefficients measured along each of the principal (*x*-, *y*- and *z*-) directions. They may differ for anisotropic diffusion. However, in the special case of perfect isotropic diffusion they are equal and ***D*** is diagonal. The eigenvalues of ***D***, i. e. $\lambda_1 \geq \lambda_2 \geq \lambda_3$, represent the magnitude of the diffusion process along the principal diffusion directions given by the eigenvectors.

DTI analysis allows calculation of the mean diffusivity (*MD*)

$$MD = \frac{\lambda_1 + \lambda_2 + \lambda_3}{3} = \frac{trace}{3}$$

which essentially corresponds to the *ADC*.

Another commonly inferred metric is the fractional anisotropy (*FA*)

$$FA = \sqrt{\frac{(\lambda_1 - \lambda_2)^2 + (\lambda_1 - \lambda_3)^2 + (\lambda_2 - \lambda_3)^2}{2(\lambda_1^2 + \lambda_2^2 + \lambda_3^2)}}$$

which is a normalized measure for the degree of anisotropy ranging from 0 (isotropic) to 1 (anisotropic). *FA* is rotationally invariant, though the orientation information can be visualized in a color-coded *FA* map, where the orientation of the main eigenvector defines the hue and *FA* the brightness. Fiber trajectories can be computed by following the primary eigenvector in each voxel.

Within the prostate fibromuscular stroma, coherently oriented myocytes have been described to lead to a distinct diffusion anisotropy, while diffusion in the glandular epithelium and lumen spaces appears to be more isotropic [15, 23, 25]. Various studies investigated the potential of *MD* and *FA* in the detection of PCa, reporting a decrease of *MD* in PCa and inconsistent results regarding *FA* [27]. *FA* variations might partly be attributed to method variations and its sensitivity to noise. Additionally, it is expected that incoherent smooth muscle orientation within a voxel at the clinically achievable level of resolution would reduce the measured *FA* [15].

Gholizadeh et al. performed DTI tractography analysis in PCa patients with perineural invasion and found a statistically significant increase in fiber tract density consistent with increased neuronal fiber density findings in PCa biopsies and their association with cancer aggressiveness [27].

## Intravoxel incoherent motion (IVIM)

In 1988, Le Bihan introduced the concept of IVIM to describe the microscopic translation of water molecules within a given voxel during an MRI experiment [28]. While at high *b*-values, the IVIM-induced signal loss is mainly caused by diffusion, at low b-values ($\leq 200\ s/mm^2$) capillary perfusion also contributes to signal attenuation (▶ **Fig. 3**). Mathematically, this can be expressed in the following biexponential model

$$S(b) = S_0 \cdot (1 - f) \cdot e^{-b \cdot D} + S_0 \cdot f \cdot e^{-b \cdot (D^* + D)}$$

where $f$ is the perfusion fraction, $D$ the molecular diffusion coefficient within the extravascular space and $D^*$ the so-called pseudo-diffusion coefficient that reflects dephasing due to perfusion in semi-randomly organized capillaries.

Various studies have been conducted on the diagnostic utility of IVIM. While results were inconsistent, some studies reported that the perfusion-free diffusion coefficient *D* may have a better diagnostic performance than *ADC* [29]. IVIM perfusion fractions in cancerous and healthy prostate tissue vary tremendously in the literature and interestingly are not always consistent with DCE parameters or expected tumor angiogenesis [15, 30–32].

## Biexponential model (BE)

At *b*-values ≥ 200–400 $s/mm^2$, IVIM effects can be considered negligible [30]. Also using a biexponential decay function, the biexponential model intends to describe the diffusion signal decay when high *b*-values ≥ 1000 $s/mm^2$ are acquired [33–35]

$$S(b) = S_0 \cdot f_{slow} \cdot e^{-b \cdot D_{slow}} + S_0 \cdot f_{fast} \cdot e^{-b \cdot D_{fast}}$$

where $D_{slow}$ and $D_{fast}$ represent the diffusion coefficients of basically two distinct diffusion environments in slow exchange with $f_{slow}$ and $f_{fast}$ as their respective fractions. In order to not confuse the biexponential approach of the IVIM model with the non-Gaussian BE model, Iima and Le Bihan suggested thinking of triexponential or exponential-polynomial models when taking IVIM and non-Gaussian diffusion altogether [30].

Great care must be taken to assign the two diffusion environments of the BE model to specific tissue compartments, especially to the intra- and extracellular space [36]. A weak correlation between the obtained volume fractions of such compartments and the relative intensities of the BE model components has been shown [36].

Studies on the detection of PCa using the BE model yielded contradictory results regarding the diagnostic significance of the BE parameters with $D_{slow}$, $D_{fast}$ and $f_{fast}$ being lower in PCa than normal tissue. In most studies the BE model was not considered superior to the *ADC* model in evaluating the aggressiveness of PCa [22].

## Diffusion kurtosis imaging (DKI)

With increasing diffusion weighting, non-Gaussian diffusion behavior becomes more evident (▶ **Fig. 3**). To quantify the deviation from the monoexponentional signal attenuation at high *b*-values (≥ 1000 $s/mm^2$), the kurtosis of the diffusion displacement probability distribution, denoted by the dimensionless parameter *K*, can be assessed. The DKI model, described by Jensen et al. in 2005, is represented by the following equation

$$S(b) = S_0 e^{-b \cdot D_K + \frac{b^2 \cdot D_K^2 \cdot K}{6}}$$

Where $D_K$ is the diffusion coefficient corrected for kurtosis [37].

Numerous studies have shown the diagnostic value of DKI parameters, although there is still no clear evidence of a diagnostic benefit compared to the ADC model. In a systematic review/meta-analysis published in 2019, Brancato et al. [22] were able to demonstrate a significant positive correlation between *K* and the Gleason score and a significant negative correlation between $D_K$ and the Gleason score. They argued that the significantly lower values of $D_K$ in PCa, particularly in intermediate to high grade lesions, may be related to the progressive destruction of the prostatic structure-like acini and an increasingly higher cellular and stroma density. The significantly higher *K*-value in intermediate to high-grade lesions, indicating reduced water diffusion, could be associated with an increasing microstructural complexity [22].

## Computed high b-value using phenomenological DWI models

DW images obtained at ultra-high *b*-values play a crucial role in tumor detection and localization [38]. In routine clinical practice, however, the use of higher *b*-values is limited by decreasing SNR due to long gradient pulses, magnetic field inhomogeneities, long echo times, motion artifacts but also economic factors as acquisition time increases. Thus, several studies investigated approaches to compute such ultra-high *b*-value DW images from low to intermediate *b*-value scans, most utilizing the ADC model

to extrapolate the high *b*-value DWI data [39], although DKI and IVIM have also been applied. Current guidelines of the German Radiological Society jointly with the professional association of German radiologists allow calculated *b*-values ≥ $s/mm^2$ analogous to measured *b*-values as certified MRI protocols for the clinical routine [40]. By avoiding the above-mentioned artifacts at ultra-high *b*-values, such reconstructions basically reduce noise and thus improve image quality, potentially enhancing lesion contrast and conspicuity in PCa [15]. As the computed ultra-high *b*-value DW images are not equivalent to actually acquired DW images at ultra-high *b*-values and contain no additional information, Shafiee et al. suggested referring to these model-based techniques as "apparent ultra-high *b*-value DWI" [41].

## Further advances in DWI – structural models

Phenomenological model parameters lack specificity, thus motivating the development of more descriptive tissue models that relate microstructural features, such as cell size and density, directly to the signal. Over the last two decades, various compartment models have been investigated in an attempt to establish a link between specific model components and diagnostic tissue characteristics [42]. Lastly, we want to introduce two promising models already applied to PCa.

### Vascular, Extracellular, and Restricted Diffusion for Cytometry in Tumors (VERDICT)

The VERDICT framework by Panagiotaki et al. [43] describes the diffusion signal arising from basically three separate water compartments without exchange: the vascular ($S_1$), extracellular-extravascular (EES, $S_2$) and intracellular (IC, $S_3$) space.

Mathematically, VERDICT is the sum of 3 parametric models:

$$S = \sum_{i=1}^{3} f_i S_i$$

where $f_i$ is the proportion of signal with no diffusion weighting from water molecules within the respective population *i*, $0 \le f_i \le 1$, $\sum_{i=1}^{3} f_i = 1$.

For the PCa tumor model, the vascular space is modeled by cylinders of uniformly distributed orientation and zero diameter, the EES by an isotropic diffusion tensor model, and the IC space by an impermeable sphere, thereby addressing the diffusion time dependency of the DWI signal within restricted compartments [44]. To minimize fitting error, the diffusion coefficients of the EES and IC space as well as the pseudo-diffusivity of the vascular space are fixed. VERDICT enables estimates of volume fractions of the respective compartments and provides a measure of cell density by $f_{IC}/R^3$, where *R* is the estimated cell radius of the sphere model [44].

In an *in vivo* pilot study, VERDICT yielded qualitatively good discrimination of benign and cancerous regions, allowing more specific insights into tissue microstructure that deciphered the various histological features underlying the changes in *ADC* and kurtosis [44]. The initially long imaging protocol has since been optimized for clinical feasibility [45].

One limitation of VERDICT is the disregard of diffusion anisotropy in the prostate.

### Restriction Spectrum Imaging (RSI)

RSI by White et al. is a linear reconstruction and modeling technique for multidimensional, i. e. multidirectional, multi *b*-value, diffusion data that provides an efficient tool for investigating tissue orientation structures over a range/"spectrum" of length scales with minimal assumptions on the underlying microarchitecture [46]. RSI is a straightforward extension of the linear spherical deconvolution model [47] that writes the oriented component of the diffusion signal as a linear mixture of cylindrically symmetric Gaussian response functions with increasing fixed transverse diffusivity and unknown volume fraction and orientation distribution. Mathematically, this can be expressed as:

$$S(b) = S_0 e^{-b \cdot (\sum_i D_i)}$$

$$D_i = (D_{\parallel} - D_{\perp}^{(i)}) \cos^2\alpha + D_{\perp}^{(i)}$$

where $D_{\parallel}$ and $D_{\perp}$ represent the longitudinal and transverse diffusivities of a cylindrically symmetric tissue element, respectively, with $D_{\parallel} > D_{\perp}$. $\alpha$ is the measurement angle relative to the cylinder axis. Two additional isotropic terms are included, one modeling "restricted" diffusion with $D_{\parallel} = D_{\perp} = 0\ mm^2/s$ and one free diffusion with $D_{\parallel} = D_{\perp} = 3 \cdot 10^{-3}\ mm^2/s$. RSI has shown great promise for PCa detection and localization [48]. An abbreviated protocol combining RSI with T2w scans may provide a viable, clinically feasible option for imaging-based PCa screening [10, 49]. Particularly within the transition zone of the prostate, conventional DWI is limited due to benign prostatic hyperplasia. RSI has demonstrated superior specificity for transition zone lesions [50].

By assuming a spectrum of Gaussian diffusion response functions, the RSI model does not account for the complex diffusion time dependency of the diffusion signal within intracellular structures. To overcome this limitation, Wichtmann et al. introduced an extension of the RSI model, called linear multi-scale modeling (LMM), which expands the RSI model by incorporating two types of response functions: a Gaussian diffusion response function [46] for hindered and free compartments and a non-Gaussian diffusion response function [51] for restricted compartments. When combined with cutting-edge acquisition techniques, the LMM framework offers a powerful, yet computationally efficient analysis method to separate orientation distributions of restricted and hindered compartments over a range of length scales, thereby allowing a more detailed characterization of tissue microstructure [52, 53].

## General considerations regarding the use of models

In principle, highly parameterized, more complex models allow a better fit of a given data set than simple models. However, models containing more parameters than can be justified by the inevitably noisy DWI data tend to overfit, resulting in high parameter

variance and poor predictive power. Conversely, a simple model such as the ADC model exhibits low parameter variance but cannot adequately capture the underlying structure of the DWI data and tends to underfit which also leads to poor predictive performance. A good model minimizes the loss of information.

Bourne et al. compared the theoretical information content of four phenomenological diffusion models in fresh and fixed prostate tissue ex vivo using the Akaike Information Criterion [36]. They found the BE and DKI model to have a higher information content than the ADC model with the BE model being superior with increasing *b*-values over ~2000 $s/mm^2$ [36]. Extending the study by Bourne et al., Liang et al. compared the theoretical information content of single and multi-compartment models in fixed prostate tissue at 9.4 T with multiple diffusion times and an extended range of b-values [54]. They noted that two-component models with an anisotropic Gaussian component and an isotropic restricted component contain the highest information value. Additionally, multi-component models were consistently more informative and reliable than single component models, irrespective of whether isotropic (ADC) or anisotropic (DTI) [54].

Furthermore, the question arises whether the additional parameters of the above described phenomenological models have any physical significance with respect to the microstructure of the examined prostate tissue [36]. As the information content may be allocated to different parameters, it is important to evaluate the relative diagnostic value of models including all their parameters and to correlate not just individual parameters but combinations with pathology [15].

Overall, models that contain both anisotropic and restricted components appear to provide a more information-rich description of DWI signals in prostate tissue than single or multi-component anisotropic models and models that do not account for restricted diffusion [54].

## Conclusion

DWI is an emerging, very powerful MRI technique to assess PCa. Although the current standard ADC model has already demonstrated a clinical benefit, it represents an oversimplification of the complexity of prostate tissue. Recent developments of DWI techniques promise increased accuracy and more specific statements about microstructural changes in malignant prostate tissue. However, extensive reproducibility and validation multi-center studies are required before being able to reliably translate these advanced approaches into the standard clinical care of PCa.


### Funding

Bundesministerium für Bildung und Forschung (13GW0388A).


### Conflict of Interest

Ulrike I. Attenberger: Industry partnership Siemens Speaker Department of Radiology and Nuclear Medicine, University Medical Center Mannheim: Research Agreement with Siemens

### References


[1] Robert-Koch-Institut und die Gesellschaft der epidemiologischen Krebsregister in Deutschland e. V., Hrsg. Krebs in Deutschland für 2015/2016. Berlin, 2019; 12. Aufl. doi:10.25646/5977

[2] Leitlinienprogramm Onkologie (Deutsche Krebsgesellschaft, Deutsche Krebshilfe, AWMF). Interdisziplinäre Leitlinie der Qualität S3 zur Früherkennung, Diagnose und Therapie der verschiedenen Stadien des Prostatakarzinoms, Langversion 5.1, AWMF Registernummer: 043/022OL. 2019 https://www.leitlinienprogramm-onkologie.de/leitlinien/prostatakarzinom/; Stand 22nd of February 2020

[3] Bott SR, Birtle AJ, Taylor CJ et al. Prostate cancer management: (1) an update on localised disease. Postgrad Med J 2003; 79: 575–580. doi:10.1136/pmj.79.936.575

[4] American College of Radiology. Prostate Imaging – Reporting and Data System, PI-RADS v2.1. American College of Radiology website: www.acrorg/Quality-Safety/Resources/PIRADS 2019; Stand 6th of January 2020

[5] Turkbey B, Rosenkrantz AB, Haider MA et al. Prostate Imaging Reporting and Data System Version 2.1: 2019 Update of Prostate Imaging Reporting and Data System Version 2. Eur Urol 2019; 76: 340–351. doi:10.1016/j.eururo.2019.02.033

[6] Franiel T, Quentin M, Mueller-Lisse UG et al. MRI of the Prostate: Recommendations on Patient Preparation and Scanning Protocol. Rofo 2017; 189: 21–28. doi:10.1055/s-0042-119451

[7] Wegelin O, van Melick HHE, Hooft L et al. Comparing Three Different Techniques for Magnetic Resonance Imaging-targeted Prostate Biopsies: A Systematic Review of In-bore versus Magnetic Resonance Imaging-transrectal Ultrasound fusion versus Cognitive Registration. Is There a Preferred Technique? Eur Urol 2017; 71: 517–531. doi:10.1016/j.eururo.2016.07.041

[8] Siddiqui MM, Rais-Bahrami S, Turkbey B et al. Comparison of MR/ultrasound fusion-guided biopsy with ultrasound-guided biopsy for the diagnosis of prostate cancer. JAMA 2015; 313: 390–397. doi:10.1001/jama.2014.17942

[9] van der Leest M, Cornel E, Israel B et al. Head-to-head Comparison of Transrectal Ultrasound-guided Prostate Biopsy Versus Multiparametric Prostate Resonance Imaging with Subsequent Magnetic Resonance-guided Biopsy in Biopsy-naive Men with Elevated Prostate-specific Antigen: A Large Prospective Multicenter Clinical Study. Eur Urol 2019; 75: 570–578. doi:10.1016/j.eururo.2018.11.023

[10] White NS, McDonald C, Farid N et al. Diffusion-weighted imaging in cancer: physical foundations and applications of restriction spectrum imaging. Cancer Res 2014; 74: 4638–4652. doi:10.1158/0008-5472.CAN-13-3534

[11] Amboss Medizinwissen. Prostatakarzinom. https://amboss.miamed.de; Stand 22nd of February 2020

[12] Le Bihan D. Apparent diffusion coefficient and beyond: what diffusion MR imaging can tell us about tissue structure. Radiology 2013; 268: 318–322. doi:10.1148/radiol.13130420

[13] Vargas HA, Lawrence EM, Mazaheri Y et al. Updates in advanced diffusion-weighted magnetic resonance imaging techniques in the evaluation of prostate cancer. World J Radiol 2015; 7: 184–188. doi:10.4329/wjr.v7.i8.184

[14] Stejskal EO, Tanner JE. Spin diffusion measurements: spin echoes in the presence of a time-dependent field gradient. The journal of chemical physics 1965; 42: 288–292

[15] Bourne R, Panagiotaki E. Limitations and Prospects for Diffusion-Weighted MRI of the Prostate. Diagnostics (Basel) 2016; 6: doi:10.3390/diagnostics6020021

[16] Nicholson C, Sykova E. Extracellular space structure revealed by diffusion analysis. Trends Neurosci 1998; 21: 207–215. doi:10.1016/s0166-2236(98)01261-2

[17] Jones DK. Diffusion MRI. Oxford University Press. 2010

[18] Stanisz GJ. Diffusion MR in biological systems: tissue compartments and exchange. Israel journal of chemistry 2003; 43: 33–44

[19] Einstein A. On the motion required by the molecular kinetic theory of heat of small particles suspended in a stationary liquid. Annalen der Physik 1905; 17: 549–560

[20] Gibbs P, Liney GP, Pickles MD et al. Correlation of ADC and T2 measurements with cell density in prostate cancer at 3.0 Tesla. Invest Radiol 2009; 44: 572–576. doi:10.1097/RLI.0b013e3181b4c10e

[21] Kim CK, Park BK, Han JJ et al. Diffusion-weighted imaging of the prostate at 3 T for differentiation of malignant and benign tissue in transition and peripheral zones: preliminary results. J Comput Assist Tomogr 2007; 31: 449–454. doi:10.1097/01.rct.0000243456.00437.59

[22] Brancato V, Cavaliere C, Salvatore M et al. Non-Gaussian models of diffusion weighted imaging for detection and characterization of prostate cancer: a systematic review and meta-analysis. Sci Rep 2019; 9: 16837. doi:10.1038/s41598-019-53350-8

[23] Bourne RM, Kurniawan N, Cowin G et al. Microscopic diffusivity compartmentation in formalin-fixed prostate tissue. Magn Reson Med 2012; 68: 614–620. doi:10.1002/mrm.23244

[24] Bourne RM, Kurniawan N, Cowin G et al. Microscopic diffusion anisotropy in formalin fixed prostate tissue: preliminary findings. Magn Reson Med 2012; 68: 1943–1948. doi:10.1002/mrm.24179

[25] Chatterjee A, Watson G, Myint E et al. Changes in Epithelium, Stroma, and Lumen Space Correlate More Strongly with Gleason Pattern and Are Stronger Predictors of Prostate ADC Changes than Cellularity Metrics. Radiology 2015; 277: 751–762. doi:10.1148/radiol.2015142414

[26] Basser PJ, Mattiello J, LeBihan D. Estimation of the effective self-diffusion tensor from the NMR spin echo. J Magn Reson B 1994; 103: 247–254. doi:10.1006/jmrb.1994.1037

[27] Gholizadeh N, Greer PB, Simpson J et al. Characterization of prostate cancer using diffusion tensor imaging: A new perspective. Eur J Radiol 2019; 110: 112–120. doi:10.1016/j.ejrad.2018.11.026

[28] Le Bihan D, Breton E, Lallemand D et al. Separation of diffusion and perfusion in intravoxel incoherent motion MR imaging. Radiology 1988; 168: 497–505. doi:10.1148/radiology.168.2.3393671

[29] Zhang YD, Wang Q, Wu CJ et al. The histogram analysis of diffusion-weighted intravoxel incoherent motion (IVIM) imaging for differentiating the gleason grade of prostate cancer. Eur Radiol 2015; 25: 994–1004. doi:10.1007/s00330-014-3511-4

[30] Iima M, Le Bihan D. Clinical Intravoxel Incoherent Motion and Diffusion MR Imaging: Past, Present, and Future. Radiology 2016; 278: 13–32. doi:10.1148/radiol.2015150244

[31] Pang Y, Turkbey B, Bernardo M et al. Intravoxel incoherent motion MR imaging for prostate cancer: an evaluation of perfusion fraction and diffusion coefficient derived from different b-value combinations. Magn Reson Med 2013; 69: 553–562. doi:10.1002/mrm.24277

[32] Dopfert J, Lemke A, Weidner A et al. Investigation of prostate cancer using diffusion-weighted intravoxel incoherent motion imaging. Magn Reson Imaging 2011; 29: 1053–1058. doi:10.1016/j.mri.2011.06.001

[33] Niendorf T, Dijkhuizen RM, Norris DG et al. Biexponential diffusion attenuation in various states of brain tissue: implications for diffusion-weighted imaging. Magn Reson Med 1996; 36: 847–857. doi:10.1002/mrm.1910360607

[34] Assaf Y, Cohen Y. Non-mono-exponential attenuation of water and N-acetyl aspartate signals due to diffusion in brain tissue. J Magn Reson 1998; 131: 69–85. doi:10.1006/jmre.1997.1313

[35] Mulkern RV, Gudbjartsson H, Westin CF et al. Multi-component apparent diffusion coefficients in human brain. NMR Biomed 1999; 12: 51–62. doi:10.1002/(sici)1099-1492(199902)12:1<51::aid-nbm546>3.0.co;2-e

[36] Bourne RM, Panagiotaki E, Bongers A et al. Information theoretic ranking of four models of diffusion attenuation in fresh and fixed prostate tissue ex vivo. Magn Reson Med 2014; 72: 1418–1426. doi:10.1002/mrm.25032

[37] Jensen JH, Helpern JA, Ramani A et al. Diffusional kurtosis imaging: the quantification of non-gaussian water diffusion by means of magnetic resonance imaging. Magn Reson Med 2005; 53: 1432–1440. doi:10.1002/mrm.20508

[38] Maas MC, Futterer JJ, Scheenen TW. Quantitative evaluation of computed high B value diffusion-weighted magnetic resonance imaging of the prostate. Invest Radiol 2013; 48: 779–786. doi:10.1097/RLI.0b013e31829705bb

[39] Bittencourt LK, Attenberger UI, Lima D et al. Feasibility study of computed vs measured high b-value (1400 s/mm(2)) diffusion-weighted MR images of the prostate. World J Radiol 2014; 6: 374–380. doi:10.4329/wjr.v6.i6.374

[40] Berufsverband Deutscher Radiologen e. V., Deutsche Röntgengesellschaft – Gesellschaft für medizinische Radiologie e.V. Multiparametrische MRT-Untersuchung der Prostata (mpMR-Prostatografie) – Technische Vorgaben. 2018 http://www.radiologenverband.de/inhalte/2018-10-03/23/multiparametrische-mrt-untersuchung-der-prostata-mpmr-prostatografie#inhalte/2018-10-03/23/multiparametrische-mrt-untersuchung-der-prostata-mpmr-prostatografie; Stand 1st of April 2020

[41] Shafiee MJ, Haider SA, Wong A et al. Apparent Ultra-High b-Value Diffusion-Weighted Image Reconstruction via Hidden Conditional Random Fields. IEEE Trans Med Imaging 2015; 34: 1111–1124. doi:10.1109/TMI.2014.2376781

[42] Panagiotaki E, Schneider T, Siow B et al. Compartment models of the diffusion MR signal in brain white matter: a taxonomy and comparison. Neuroimage 2012; 59: 2241–2254. doi:10.1016/j.neuroimage.2011.09.081

[43] Panagiotaki E, Walker-Samuel S, Siow B et al. Noninvasive quantification of solid tumor microstructure using VERDICT MRI. Cancer Res 2014; 74: 1902–1912. doi:10.1158/0008-5472.CAN-13-2511

[44] Panagiotaki E, Chan RW, Dikaios N et al. Microstructural characterization of normal and malignant human prostate tissue with vascular, extracellular, and restricted diffusion for cytometry in tumours magnetic resonance imaging. Invest Radiol 2015; 50: 218–227. doi:10.1097/RLI.0000000000000115

[45] Panagiotaki E, Andrada I, Johnston E et al. Optimised VERDICT MRI protocol for prostate cancer characterisation. In, 23rd Annual Meeting of the International Society for Magnetic Resonance in Medicine. Toronto, Ontario, Canada, 2015; 2872

[46] White NS, Leergaard TB, D'Arceuil H et al. Probing tissue microstructure with restriction spectrum imaging: Histological and theoretical validation. Hum Brain Mapp 2013; 34: 327–346. doi:10.1002/hbm.21454

[47] Tournier JD, Calamante F, Gadian DG et al. Direct estimation of the fiber orientation density function from diffusion-weighted MRI data using spherical deconvolution. Neuroimage 2004; 23: 1176–1185. doi:10.1016/j.neuroimage.2004.07.037

[48] White NS, McDonald CR, Farid N et al. Improved conspicuity and delineation of high-grade primary and metastatic brain tumors using "restriction spectrum imaging": quantitative comparison with high B-value DWI and ADC. AJNR Am J Neuroradiol 2013; 34: 958–964, S951. doi:10.3174/ajnr.A3327

[49] Brunsing RL, Schenker-Ahmed NM, White NS et al. Restriction spectrum imaging: An evolving imaging biomarker in prostate MRI. J Magn Reson Imaging 2017; 45: 323–336. doi:10.1002/jmri.25419

[50] Felker ER, Raman SS, Shakeri S et al. Utility of Restriction Spectrum Imaging Among Men Undergoing First-Time Biopsy for Suspected Prostate Cancer. Am J Roentgenol 2019; 213: 365–370. doi:10.2214/AJR.18.20836

[51] van Gelderen P, DesPres D, van Zijl PC et al. Evaluation of restricted diffusion in cylinders. Phosphocreatine in rabbit leg muscle. J Magn Reson B 1994; 103: 255–260. doi:10.1006/jmrb.1994.1038

[52] Wichtmann BD, Huang S, Fan Q et al. Linear Multi-scale Modeling of diffusion MRI data: A framework for characterization of orientational structures across length scales. In, 24th Annual Meeting of the International Society for Magnetic Resonance in Medicine. Singapore, Singapore, 2016; 5142

[53] Wichtmann BD, Nummenmaa A, Fan Q et al. Investigating microstructural signatures for low-grade gliomas using Linear Multi-scale Modeling of diffusion MRI data. In, 25th Annual Meeting of the International Society for Magnetic Resonance in Medicine. Honolulu, HI, USA, 2017; 3362

[54] Liang S, Panagiotaki E, Bongers A et al. Information-based ranking of 10 compartment models of diffusion-weighted signal attenuation in fixed prostate tissue. NMR Biomed 2016; 29: 660–671. doi:10.1002/nbm.3510